

Lorentz Covariant Canonical Symplectic Algorithms for Dynamics of Charged Particles

Yulei Wang,^{1,2} Jian Liu,^{1,2,*} and Hong Qin^{1,3}

¹*School of Nuclear Science and Technology and Department of Modern Physics, University of Science and Technology of China, Hefei, Anhui 230026, China*

²*Key Laboratory of Geospace Environment, CAS, Hefei, Anhui 230026, China*

³*Plasma Physics Laboratory, Princeton University, Princeton, NJ 08543, USA*

Abstract

In this paper, the Lorentz covariance of algorithms is introduced. Under Lorentz transformation, both the form and performance of a Lorentz covariant algorithm are invariant. To acquire the advantages of symplectic algorithms and Lorentz covariance, a general procedure for constructing Lorentz covariant canonical symplectic algorithms (LCCSA) is provided, based on which an explicit LCCSA for dynamics of relativistic charged particles is built. LCCSA possesses Lorentz invariance as well as long-term numerical accuracy and stability, due to the preservation of discrete symplectic structure and Lorentz symmetry of the system. For situations with time-dependent electromagnetic fields, which is difficult to handle in traditional construction procedures of symplectic algorithms, LCCSA provides a perfect explicit canonical symplectic solution by implementing the discretization in 4-spacetime. We also show that LCCSA has built-in energy-based adaptive time steps, which can optimize the computation performance when the Lorentz factor varies.

* corresponding author: jliuphy@ustc.edu.cn

I. INTRODUCTION

The advanced structure-preserving geometric algorithms have stepped into the field of plasma physics and attracted more and more attentions in recent years [1–11]. Through preserving different geometric structures, such as the phase-space volume, the symplectic structure, and the Poisson structure, geometric algorithms possess long-term numerical accuracy and stability and have shown powerful capabilities in dealing with multi-scale and nonlinear problems. Volume-preserving algorithms (VPA) of different orders for both non-relativistic and relativistic full-orbit dynamics of charged particles have been constructed in several publications [12–14]. A Poisson-preserving algorithm for solving the Vlasov-Maxwell system is built through splitting the Hamiltonian and using the Morrison-Marsden-Weinstein bracket [15]. As an important aspect of geometric algorithms, symplectic methods have produced fruitful results. For gyro-center dynamics of charged particles, variational symplectic methods have been studied and applied to plasma simulations [1–3]. It is also feasible to canonicalize the gyro-center equations to construct canonical symplectic algorithms for time-independent magnetic fields [16]. The Particle-in-Cell (PIC) method, known as the first principle simulation method for plasma systems, has been reconstructed by the use of different symplectic methods, including variational symplectic method, canonical symplectic method, and non-canonical symplectic method [6–9]. Theoretically, symplectic methods impose numerical results with a set of constrains, the number of which is determined by the freedom degrees of the systems [9, 17], by preserving the global symplectic structure of the system. Correspondingly, the global relative errors of motion constants can be restricted to bounded small values, which enable symplectic algorithms to retain many key properties of the origin continuous systems. However, another essential geometric property of physical systems has long been ignored in structure-preserving algorithms, i.e., the Lorentz covariance. The lack of Lorentz covariance leads to inconsistent numerical solutions in different inertial frames. In this paper, we equip the symplectic algorithm with the Lorentz covariance to obtain better performances.

As an intrinsic property of continuous physical systems, the Lorentz covariance has become a common sense in modern physics, which states that the physical rules and events keep invariant under Lorentz transformation [18]. It is also important for algorithms to satisfy the Lorentz covariance. Similar to continuous covariant system, Lorentz covariant algorithms

have invariant forms and describe invariant processes under Lorentz transformation. The Lorentz invariance of each one-step map ensures the reference-independence of numerical results, which leads to that the numerical properties, such as stability, convergence, and consistency are also independent with the choice of reference frames. In applications, the Lorentz covariant algorithms make it convenient and safe to adopt the same set of discretized equations in all inertial frames.

The combination of Lorentz covariance and symplectic method can generate algorithms possessing benefits from the both. If the long-term numerical accuracy and stability are unavailable, Lorentz covariant algorithms cannot guarantee the long-term correctness of simulations, even though the results are reference-independent. On contrary, although symplectic methods without Lorentz covariance have long-term conservativeness and stability, they break the Lorentz symmetry of the original continuous systems and produce inconsistent numerical solutions in different inertial frames. On the other hand, it is difficult to construct conventional symplectic algorithms for time-dependent Hamiltonian systems. Meanwhile, it is not straightforward to develop conventional symplectic algorithms with optimized adaptive time steps. These two problems can be solved automatically by the construction of Lorentz covariant symplectic algorithms. Covariant algorithms directly iterate geometric objects in 4-spacetime and discretize the worldlines with respect to the discrete proper time τ . Consequently, the time, t , as a component of the 4-spacetime, plays the same role as spatial coordinates in time-dependent Hamiltonians. Taking the place of t , the proper time is employed as the dynamical parameter and leads to proper-time-independent Hamiltonians for time-dependent systems. Because covariant algorithms directly discretize the worldline, one can obtain energy-based adaptive-time-step symplectic schemes given the fixed proper-time step $\Delta\tau = \Delta t/\gamma$. The adaptive time step can improve the performance of symplectic algorithms when the Lorentz factor varies.

To endue symplectic algorithms with Lorentz covariance, a straightforward way is to start from the view point of geometry. The Lorentz covariant systems reside in the 4-dimensional spacetime. Considering the reference-independence, the Lorentz covariant discretized equations can be regarded as the one-step maps of geometric objects in spacetime. As a result, if one starts from covariant continuous geometric equations, and discretizes these equations without breaking the integrity of all the geometric objects, the Lorentz covariance can be naturally inherited. The canonical symplectic methods directly deal with the Hamil-

tonian equations of physical systems. During discretization, the symplectic structure of Hamiltonian equations is retained, and each of the physical quantities is treated as an inseparable discretized geometric object, updated at different proper-time steps [17]. It is readily to see that the canonical symplectic method provides a convenient way to combine the symplectic method and the Lorentz covariance. Here we summarize a general procedure for constructing Lorentz covariant canonical symplectic algorithms (LCCSA), namely, 1) to write down the covariant geometric Hamiltonian equation for a target physical system in 4-dimensional spacetime, 2) to discretize the Hamiltonian equations by using a canonical symplectic scheme, such as Euler-symplectic scheme and implicit mid-point symplectic scheme, described by geometric objects in 4-spacetime.

Following this procedure, we construct an explicit LCCSA for the simulation of relativistic dynamics of charged particles. Compared with a non-covariant algorithm, LCCSA exhibits the reference-independent form and good long-term performances in different Lorentz frames. As a symplectic algorithm, LCCSA shows outstanding long-term numerical accuracy than a covariant fourth-order Runge-Kutta algorithm (RK4). Meanwhile, LCCSA can automatically adjust the time step-length according to the energy of a particle and guarantee the approximate constant time-sampling number in one gyro-period. The performance in simulating energy-changing processes can be improved. As examples, both the computation efficiency for simulating acceleration and braking processes of charged particle by use of LCCSA are optimized compared with those fixed-time-step algorithms.

The rest part of this paper is organized as follows. The definition and properties of Lorentz covariant symplectic algorithms are introduced in Sec. II. The detailed procedure of constructing an explicit LCCSA is explained in Sec. III. In Sec. IV, the performances of LCCSA are exhibited through several typical numerical cases. We summarize this article in Sec. V.

II. LORENTZ COVARIANT SYMPLECTIC ALGORITHMS

Before introducing Lorentz covariant symplectic algorithms, we first provide the rigorous definition of Lorentz covariant algorithm. For a given continuous Lorentz covariant system \mathbf{F} , an algorithm A is called Lorentz covariant if and only if it satisfies

$$\mathcal{D}_A \circ \mathcal{T}_L \mathbf{F} = \mathcal{T}_L \circ \mathcal{D}_A \mathbf{F}, \quad (1)$$

where \mathcal{T}_L denotes the Lorentz transformation operator, \mathcal{D}_A denotes the discretization operator determined by the algorithm A , the operation “ \circ ” means composite mapping, and L denotes the Lorentz transformation matrix satisfying $L^T g L = g$, where g is the Lorentz metric tensor of the 4-dimensional spacetime [18–20]. Generally speaking, L can be both proper Lorentz transformation ($\det L = +1$) and improper Lorentz transformation ($\det L = -1$). A Lorentz transformation includes the rotation and the Lorentz boost of inertial frames [18]. Suppose that A is applied to system \mathbf{F} in the inertial frame \mathcal{O} , the first operation on the right-hand side of Eq. 1, $\phi_A = \mathcal{D}_A \mathbf{F}$, gives a realization of algorithm A , i.e., a set of discrete equations in this frame. In another inertial frame \mathcal{O}' moving with speed β relative to \mathcal{O} , this discrete system are described by discrete equations $\phi'_A = \mathcal{T}_L \phi_A$ following the Lorentz transformation of ϕ_A . On the left-hand side of Eq. 1, because the original system \mathbf{F} is Lorentz covariant, $\mathbf{F}' = \mathcal{T}_L \mathbf{F}$ takes the same form as \mathbf{F} . Consequently, the realization of algorithm A on \mathbf{F}' , i.e., $\xi_A = \mathcal{D}_A \mathbf{F}'$, also takes the same form as ϕ_A except that the physical quantities in ξ_A are observed in the frame \mathcal{O}' . So Eq. 1 concludes that the discrete equations generated by a Lorentz covariant algorithm A have the invariant form and provides the same discretized system in different Lorentz inertial frames.

To make the picture of covariant algorithms clearer, for comparison, we investigate an example of a non-covariant algorithm, i.e., the VPA for relativistic charged particles dynamics as constructed in [13]. This algorithm has been applied to the study of long-term dynamics of runaway electrons in tokamaks and shown its outstanding long-term numerical accuracy [10, 11]. However, its non-Lorentz-covariant property can be proved according to Eq. 1 as follows. The target continuous system is the relativistic Lorentz force equations \mathbf{F}_{L3}

$$\frac{d\mathbf{x}}{dt} = \frac{\mathbf{p}}{\gamma}, \quad (2)$$

$$\frac{d\mathbf{p}}{dt} = \mathbf{E} + \frac{\mathbf{p} \times \mathbf{B}}{\gamma}, \quad (3)$$

where \mathbf{x} is the position, \mathbf{p} is the mechanical momentum, $\gamma = \sqrt{1 + p^2}$ is the Lorentz factor, and \mathbf{E} and \mathbf{B} are respectively electric and magnetic fields. Notice that all the physical quantities in this paper are normalized according to Tab. I unless noted otherwise. As a common wisdom, \mathbf{F}_{L3} is Lorentz covariant. We will show that $\mathcal{D}_{VPA} \circ \mathcal{T}_L \mathbf{F}_{L3} \neq \mathcal{T}_L \circ \mathcal{D}_{VPA} \mathbf{F}_{L3}$.

Firstly, we derive the discrete system $\phi'_{VPA} = \mathcal{T}_L \circ \mathcal{D}_{VPA} \mathbf{F}_{L3}$. In the reference frame \mathcal{O} , by applying the discrete operator to \mathbf{F}_{L3} we obtain $\phi_{VPA} = \mathcal{D}_{VPA} \mathbf{F}_{L3}$, which is a set of

Names	Symbols	Units
Time, Proper Time, Gyro-period	t, τ, T_{ce}	m_0/eB_0
Position	\mathbf{x}	m_0c/eB_0
Mechanical/Canonical Momentum	\mathbf{p}, \mathbf{P}	m_0c
Velocity	$\mathbf{v}, \boldsymbol{\beta}$	c
Electric field	\mathbf{E}	B_0c
Magnetic field	\mathbf{B}	B_0
Vecter field	\mathbf{A}	e/m_0c
Scalar field	ϕ	e/m_0c^2
Hamiltonian	\mathcal{H}	m_0c^2

Table I. Units of all the physical quantities used in this paper. m_0 is the rest mass of a particle, e is the elementary charge, c is the speed of light, and B_0 is the given reference magnetic field.

difference equations in \mathcal{O} and can be written explicitly as [13],

$$t_{k+1} = t_k + \Delta t, \quad (4)$$

$$\mathbf{x}_{k+1} = \mathbf{x}_k + \Delta t \frac{\mathbf{p}_k}{\gamma_k}, \quad (5)$$

$$\mathbf{p}_{k+1} = \mathbf{p}_k + \mathbf{W}, \quad (6)$$

where $\gamma_k = \sqrt{1 + p_k^2}$, and $\mathbf{W}(t_{k+1}, \mathbf{x}_{k+1}, \mathbf{p}_k, \mathbf{E}_{k+1}, \mathbf{B}_{k+1}, \Delta t)$ is a function given by

$$\mathbf{W} = \Delta t \mathbf{E}_{k+1} + \left(D \hat{\mathbf{B}}_{k+1} + d D \hat{\mathbf{B}}_{k+1}^2 \right) \left(\mathbf{p}_k + \frac{\Delta t}{2} \mathbf{E}_{k+1} \right), \quad (7)$$

where $\mathbf{E}_{k+1} = \mathbf{E}(t_{k+1}, \mathbf{x}_{k+1})$, $\mathbf{B}_{k+1} = \mathbf{B}(t_{k+1}, \mathbf{x}_{k+1})$, $d = \Delta t / \left[2\sqrt{1 + (\mathbf{p}_k + \Delta t \mathbf{E}_{k+1}/2)^2} \right]$, and $D = 2d / \left(1 + d^2 B_{k+1}^2 \right)$, and in Cartesian coordinate system $\hat{\mathbf{B}}$ is defined as

$$\hat{\mathbf{B}} = \begin{pmatrix} 0 & B_z & -B_y \\ -B_z & 0 & B_x \\ B_y & -B_x & 0 \end{pmatrix}. \quad (8)$$

Then, we transform ϕ_{VPA} into another frame \mathcal{O}' . We suppose that \mathcal{O}' moves with a fixed speed $\boldsymbol{\beta} = (\beta_1, \beta_2, \beta_3)$ relative to \mathcal{O} . In this case, the Lorentz matrix L denotes the Lorentz

boost matrix which can be written explicitly in the Cartesian coordinate system as,

$$L = \begin{pmatrix} \Gamma & -\Gamma\beta_1 & -\Gamma\beta_2 & -\Gamma\beta_3 \\ -\Gamma\beta_1 & 1 + \frac{(\Gamma-1)\beta_1^2}{\beta^2} & \frac{(\Gamma-1)\beta_1\beta_2}{\beta^2} & \frac{(\Gamma-1)\beta_1\beta_3}{\beta^2} \\ -\Gamma\beta_2 & \frac{(\Gamma-1)\beta_1\beta_2}{\beta^2} & 1 + \frac{(\Gamma-1)\beta_2^2}{\beta^2} & \frac{(\Gamma-1)\beta_2\beta_3}{\beta^2} \\ -\Gamma\beta_3 & \frac{(\Gamma-1)\beta_1\beta_3}{\beta^2} & \frac{(\Gamma-1)\beta_2\beta_3}{\beta^2} & 1 + \frac{(\Gamma-1)\beta_3^2}{\beta^2} \end{pmatrix}, \quad (9)$$

where $\beta = |\boldsymbol{\beta}|$, and $\Gamma = 1/\sqrt{1-\beta^2}$ is the Lorentz factor of frame \mathcal{O}' . Without loss of generality, we set $\boldsymbol{\beta}$ as $(\beta, 0, 0)$. Substituting \mathbf{x}_k , \mathbf{p}_k , γ_k , Δt , \mathbf{E}_k and \mathbf{B}_k in Eq. 5 and Eq. 6 by

$$t_k = \Gamma (t'_k + \beta x'_k), \quad (10)$$

$$x_k = \Gamma (\beta t'_k + x'_k), \quad (11)$$

$$y_k = y'_k, \quad (12)$$

$$z_k = z'_k, \quad (13)$$

$$\gamma_k = \Gamma (\gamma'_k + \beta p'_{x,k}), \quad (14)$$

$$p_{x,k} = \Gamma (\beta \gamma'_k + p'_{x,k}), \quad (15)$$

$$p_{y,k} = p'_{y,k}, \quad (16)$$

$$p_{z,k} = p'_{z,k}, \quad (17)$$

$$\Delta t = \frac{\gamma_k}{\gamma'_k} \Delta t' = \frac{\Gamma (\gamma'_k + \beta p'_{x,k})}{\gamma'_k} \Delta t', \quad (18)$$

$$\mathbf{E}_k = f_E (\mathbf{E}'_k, \mathbf{B}'_k), \quad (19)$$

$$\mathbf{B}_k = f_B (\mathbf{E}'_k, \mathbf{B}'_k), \quad (20)$$

where f_E and f_B are the Lorentz transformation functions for electric and magnetic fields [18]. After simplification, the difference equations in \mathcal{O}' , $\phi'_{VPA} = \mathcal{T}_L \phi_{VPA}$, becomes

$$t'_{k+1} = t'_k + \Delta t', \quad (21)$$

$$\mathbf{x}'_{k+1} = \mathbf{x}'_k + \Delta t' \frac{\mathbf{p}'_k}{\gamma'_k}, \quad (22)$$

$$p'_{x,k+1} = p'_{x,k} + \beta \left(\sqrt{1 + (p'_k)^2} - \sqrt{1 + (p'_{k+1})^2} \right) + \frac{W'_x}{\Gamma}, \quad (23)$$

$$p'_{y,k+1} = p'_{y,k} + W'_y, \quad (24)$$

$$p'_{z,k+1} = p'_{z,k} + W'_z, \quad (25)$$

where W'_x , W'_y , and W'_z are three components of $\mathbf{W}'(t'_{k+1}, \mathbf{x}'_{k+1}, \gamma'_k, \mathbf{p}'_k, \mathbf{E}'_{k+1}, \mathbf{B}'_{k+1}, \Delta t')$ which is given by

$$\mathbf{W}' = \mathbf{W} \left[t_{k+1}(t'_{k+1}, \mathbf{x}'_{k+1}), \mathbf{x}_{k+1}(t'_{k+1}, \mathbf{x}'_{k+1}), \mathbf{p}_k(\gamma'_k, \mathbf{p}'_k), f_E, f_B, \Delta t(\gamma'_k, p'_{x,k}, \Delta t') \right]. \quad (26)$$

According to Eq. 23, ϕ'_{VPA} is an implicit scheme.

Next, we derive the difference equations determined by $\xi_{VPA} = \mathcal{D}_{VPA} \circ \mathcal{T}_L \mathbf{F}_{L3}$. Because Eqs. 2 and 3 are covariant equations, the target continuous system in frame \mathcal{O}' takes the form $\mathbf{F}'_{L3} = \mathcal{T}_L \mathbf{F}_{L3}$, i.e.,

$$\frac{d\mathbf{x}'}{dt'} = \frac{\mathbf{p}'}{\gamma'}, \quad (27)$$

$$\frac{d\mathbf{p}'}{dt'} = \mathbf{E}' + \frac{\mathbf{p}' \times \mathbf{B}'}{\gamma'}. \quad (28)$$

Discretizing \mathbf{F}'_{L3} by VPA, the difference equation $\xi_{VPA} = \mathcal{D}_{VPA} \mathbf{F}'_{L3}$ is given by

$$\mathbf{x}'_{k+1} = \mathbf{x}'_k + \Delta t' \frac{\mathbf{p}'_k}{\gamma'_k}, \quad (29)$$

$$\mathbf{p}'_{k+1} = \mathbf{p}'_k + \mathbf{V}', \quad (30)$$

where $\mathbf{V}'(t'_{k+1}, \mathbf{x}'_{k+1}, \mathbf{p}'_k, \mathbf{E}'_{k+1}, \mathbf{B}'_{k+1}, \Delta t') = \mathbf{W}(t'_{k+1}, \mathbf{x}'_{k+1}, \mathbf{p}'_k, \mathbf{E}'_{k+1}, \mathbf{B}'_{k+1}, \Delta t')$. It is obvious that $\xi_{VPA} \neq \phi'_{VPA}$. That the VPA in [13] is not Lorentz covariant is therefore proved.

Being both Lorentz covariant and symplectic, an algorithm is of significance in two aspects. In the first place, the preservation of the symplectic structure guarantees that the numerical solutions are good enough to approximate the continuous solutions in arbitrary long time. Secondly, the Lorentz covariance of algorithm makes the numerical results reference-independent, which preserves the geometric nature of original systems. Figure 1 depicts the schematic diagram for the relation between a covariant continuous system and the corresponding discrete systems generated by the Lorentz covariant symplectic algorithm A . The 4-spacetime is denoted by M_{ST} . The continuous evolution of the original system forms a worldline, marked by C_{wl} , starting from the initial condition p^0 . The reference frames \mathcal{O} and \mathcal{O}' are two chosen Lorentz inertial frames. For a covariant continuous system, the master equations \mathbf{F}' in \mathcal{O}' has identical form as \mathbf{F} in \mathcal{O} . According to the Lorentz covariance, the solutions of \mathbf{F} and \mathbf{F}' , i.e., z^τ and z'^τ , express the same worldline in M_{ST} . Given A is a covariant algorithm, the corresponding discretized equations in \mathcal{O}' is expressed as $\xi_A = \mathcal{D}_A \mathbf{F}'$,

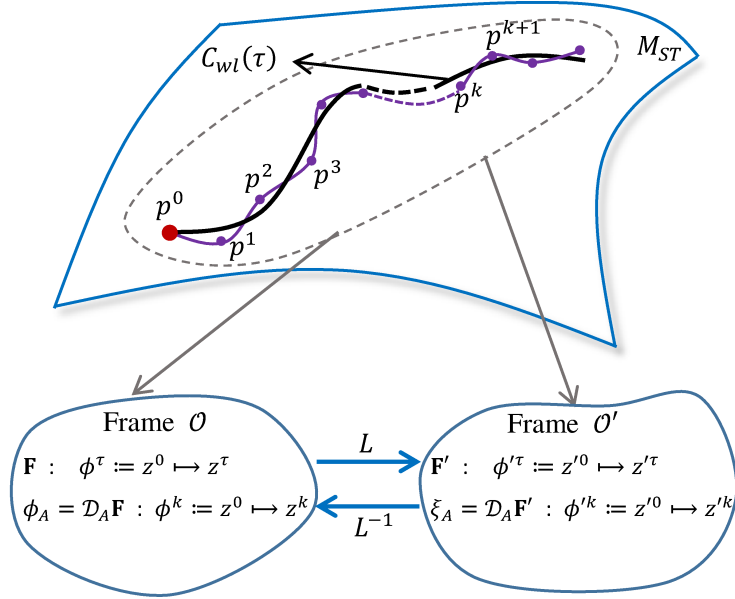


Figure 1. Schematic diagram for the covariance of continuous systems and the Lorentz covariant symplectic algorithms. M_{ST} is the configuration space of 4-spacetime. The worldline, C_{wl} , is denoted by the black solid curve. The sequence of purple points, p^k , denote the discrete approximation of C_{wl} . Two Lorentz frames, \mathcal{O} and \mathcal{O}' , are chosen to express the Lorentz transformation relations. For covariant continuous system, \mathbf{F} and \mathbf{F}' have the same form, and their solutions in different reference frames give the same worldline on M_{ST} with the initial condition p^0 . Similarly, for Lorentz covariant algorithm A , the discrete systems $\phi_A = \mathcal{D}_A \mathbf{F}$ and $\xi_A = \mathcal{D}_A \mathbf{F}'$ have the same form, and their results z^k and z'^k describe the same sequence p^k on M_{ST} , if the Lorentz transformation can be calculated exactly.

and $\phi_A = \mathcal{D}_A \mathbf{F}$ denotes the discretized equations in frame \mathcal{O} . The sequence determined by ϕ_A in \mathcal{O} is denoted by z^k , and the sequence determined by ξ_A in \mathcal{O}' is denoted by z'^k . According to Eq. 1, we have the relation $\xi_A = \mathcal{T}_L \phi_A$ and thus $z'^k = \mathcal{T}_L z^k$ for each proper-time step k . Consequently, as the analogy with the continuous case, the numerical results of A in different Lorentz frames provide different numerical solutions z^k and z'^k but the same 4-worldpoint sequence p^k in M_{ST} . On the other hand, because A is a symplectic algorithm, the conservation of discrete symplectic structure ensures p^k locates adjacent to the exact

solution of the original continuous system C_{wl} in M_{ST} , see the purple curve in Fig. 1. We can conclude that the Lorentz covariant symplectic algorithms have long-term numerical conservativeness, accuracy, and stability, which are independent of the choice of reference frames.

III. CONSTRUCTION OF LCCSA

In this section, we introduce a convenient procedure for the construction of LCCSA. The construction of an explicit LCCSA for relativistic dynamics of charged particles is introduced step by step for demonstration. This procedure can be generally applied for the construction of Lorentz covariant symplectic algorithms for any other Lorentz covariant continuous Hamiltonian systems. Since the Lorentz covariance should be preserved during the discretization, the geometric properties in 4-spacetime should be preserved. It is convenient to employ the Lorentz-covariant forms of the continuous system to construct LCCSA.

Firstly, write explicitly down the covariant Hamiltonian equations for charged particles in 4-spacetime. The covariant Hamiltonian describing charged particle dynamics in electromagnetic fields is [21]

$$H = \frac{g^{\alpha\beta} (P_\alpha - A_\alpha) (P_\beta - A_\beta)}{2}, \quad (31)$$

where X^α is the 4-position vector, P_α is the canonical momentum 1-form, and A_α denotes the 4-vector-potential 1-form. In Cartesian coordinate system, we have $X^\alpha = (t, \mathbf{x})$, $P_\alpha = (\gamma + \phi, -\mathbf{P})$, $A_\alpha = (\phi, -\mathbf{A})$, and

$$g_{\alpha\beta} = g^{\alpha\beta} = \begin{pmatrix} 1 & 0 & 0 & 0 \\ 0 & -1 & 0 & 0 \\ 0 & 0 & -1 & 0 \\ 0 & 0 & 0 & -1 \end{pmatrix},$$

where \mathbf{P} is the canonical momentum, and ϕ and \mathbf{A} are respectively the scalar and vector potentials of electromagnetic fields. Before deriving the Hamiltonian equations, one should notice that the evolution parameters should be Lorentz scalars, which is vital to keep the Lorentz invariance of step-length after discretization. As a direct consideration, we choose the proper time τ as the evolution parameter. Correspondingly, according to the Hamilto-

nian given in Eq. 31, we obtain the covariant Hamiltonian equations \mathbf{F}_{L4} [18, 21],

$$\frac{dP_\alpha}{d\tau} = -\frac{\partial H}{\partial X^\alpha} = (P^\beta - A^\beta) \partial_\alpha A_\beta, \quad (32)$$

$$\frac{dX^\alpha}{d\tau} = \frac{\partial H}{\partial P_\alpha} = P^\alpha - A^\alpha, \quad (33)$$

where $\partial_\alpha = \partial/\partial X^\alpha = (\partial/\partial X^0, \nabla)$, $P^\alpha = g^{\alpha\beta} P_\beta$, and $A^\alpha = g^{\alpha\beta} A_\beta$. It is readily to see that Eqs. 32 and 33 are geometric equations and have reference invariant forms in all Lorentz inertial frames.

Secondly, discretize the Hamiltonian equations by using a canonical symplectic method. To obtain an explicit scheme with high efficiency, here we choose the Euler-symplectic method, which can be expressed by [9, 17]

$$P^{k+1} = P^k - h \frac{\partial H}{\partial X} (P^{k+1}, X^k), \quad (34)$$

$$X^{k+1} = X^k + h \frac{\partial H}{\partial P} (P^{k+1}, X^k), \quad (35)$$

where h is the step-length. The Euler-symplectic method does not break the geometric object or the form of continuous equations. Combining Eqs. 32-35, we can obtain the discrete equations of the LCCSA $\phi_{LCCSA} = \mathcal{D}_{LCCSA} \mathbf{F}_{L4}$ as

$$P_\alpha^{k+1} = P_\alpha^k + \Delta\tau (P^{\beta,k+1} - A^{\beta,k}) \frac{\partial A_\beta^k}{\partial X^\alpha}, \quad (36)$$

$$X^{\alpha,k+1} = X^{\alpha,k} + \Delta\tau (P^{\alpha,k+1} - A^{\alpha,k}), \quad (37)$$

where $\Delta\tau$ is the step-length of proper time. The difference equations, Eqs. 36-37, act as one-step maps of geometric objects $(X^{\alpha,k}, P_\alpha^k) \mapsto (X^{\alpha,k+1}, P_\alpha^{k+1})$. As a property of geometric equations, Eqs. 36-37 naturally inherit the reference-independence of Eqs. 32-33. The Lorentz covariance of the LCCSA can also be verified directly through the definition Eq. 1. The Lorentz transformation of ϕ_{LCCSA} , $\phi'_{LCCSA} = \mathcal{T}_L \phi_{LCCSA}$, can be given by left-multiplying the Lorentz matrix on both sides of Eqs. 36 and 37. Considering the linear relations of all the terms in Eqs. 36-37, it is obvious to see that ϕ'_{LCCSA} has the same form with $\xi_{LCCSA} = \mathcal{D}_{LCCSA} \circ \mathcal{T}_L \mathbf{F}_{L4}$. Therefore, LCCSA satisfies the definition of Lorentz covariant algorithms.

During discretization, the Lorentz covariance cannot be inherited without keeping geometric objects in 4-spacetime, even though the 4-dimensional covariant Hamiltonian equations are used. To explain this, we provide a counter-example, a non-covariant algorithm

(NCOVA) of Eqs. 32-33, namely, ϕ_{NCOVA} ,

$$P_\alpha^{k+1} = P_\alpha^k + \Delta\tau \left(P^{\beta,k} - A^{\beta,k} \right) \partial_\alpha A_\beta^k, \quad (38)$$

$$X^{0,k+1} = X^{0,k} + \Delta\tau \left(P^{0,k+1} - A^{0,k} \right), \quad (39)$$

$$\mathbf{x}^{k+1} = \mathbf{x}^k + \Delta\tau \left(\mathbf{P}^k - \mathbf{A}^k \right), \quad (40)$$

where X^0 , P^0 , and A^0 denote the 0-components of X^α , P^α , and A^α , respectively. The one-step map of P_α determined by Eq. 38 is the Euler method. In Eqs. 39-40, the 4-canonical-momentum for pushing X^α is treated in different ways. When calculating $X^{0,k+1}$, $P^{0,k+1}$ is used. And \mathbf{P}^k is used to calculate \mathbf{x}^{k+1} . The integrity of 4-dimensional 1-form P_α in Eq. 33 is thus broken, which lead to different forms of Eqs. 39-40 after Lorentz transformations. The bad performance of this NCOVA under Lorentz transformation is presented in numerical examples in Sec. IV, which shows numerically that $\mathcal{T}_L \phi_{NCOVA} \neq \xi_{NCOVA}$, where $\xi_{NCOVA} = D_{NCOVA} \circ \mathcal{T}_L \mathbf{F}_{L^4}$.

IV. NUMERICAL EXPERIMENTS

In this section, we analyze and test the performances of LCCSA through several numerical experiments.

A. The Lorentz covariance

To test the Lorentz covariance of algorithms, the motion of an electron is simulated in different Lorentz frames. The background magnetic field is given by

$$\mathbf{B} = B_0 \frac{R}{R_0} \mathbf{e}_z, \quad (41)$$

which has the vector potential

$$\mathbf{A} = B_0 \frac{R^2}{3R_0} \mathbf{e}_\theta, \quad (42)$$

where $R = \sqrt{x^2 + y^2}$, \mathbf{e}_z and \mathbf{e}_θ are the unit vectors of cylindrical coordinates. The parameters of field are set as $B_0 = 1 \text{ T}$ and $R_0 = m_0 c / e B_0 \approx 1.69 \times 10^{-3} \text{ m}$. We mark the lab reference frame as \mathcal{O} , where the initial condition of the charged particle is set as $\mathbf{x}_0 = (0, 2R_0, 0)$ and $\mathbf{p}_0 = (0, m_0 c, 0)$. We then find another frame \mathcal{O}' moves with velocity

$\beta_{cor} = (0.5, 0, 0)$ relative to \mathcal{O} . Initially, the local time of the \mathcal{O} and \mathcal{O}' are both set to be 0, and the origin points of \mathcal{O} and \mathcal{O}' coincide in 4-spacetime.

In the case of LCCSA, we first apply ξ_{LCCSA} in \mathcal{O}' . Once obtained the numerical solution $\mathbf{z}'_{\xi}{}^k$ in \mathcal{O}' , we transform it back to the frame \mathcal{O} to get the result of $\mathbf{z}_{\xi}^k = \mathcal{T}_{L^{-1}} \circ \xi_{LCCSA} \mathbf{z}'{}^0$, where $\mathbf{z} = (\mathbf{x}, \mathbf{p})$. On the other hand, by using ϕ_{LCCSA} , we can get discrete solution $\mathbf{z}_{\phi}^k = \phi_{LCCSA} \mathbf{z}^0$ in \mathcal{O} directly. The orbits of the electron in the x-y plane are plotted in Fig. 2, and the difference between the x-components of \mathbf{z}_{ϕ}^k and \mathbf{z}_{ξ}^k is denoted by $D_x^k = x_{\phi}^k - x_{\xi}^k$. It can be observed that the numerical difference comes from calculations in different Lorentz frames is about 10^{-15} m, which is in the order of machine precision. Meanwhile, D_x^k is nearly independent with the step-length, see Figs. 2c and Figs. 2f. It is shown in Fig. 2 that the difference equations of LCCSA in \mathcal{O} and \mathcal{O}' , namely, ϕ_{LCCSA} and ξ_{LCCSA} , can produce the same results if the numerical error caused by the calculation of Lorentz transformation is neglected. As a result, the stability, convergence, and consistency of LCCSA are reference independent, which makes it safe to use LCCSA directly in different frames.

For comparison, the relativistic VPA and NCOVA are also used to calculate the same case. Because VPA is not a covariant algorithm as discussed in Sec. II, if we calculate the dynamics of a charged particle in \mathcal{O}' by use of ξ_{VPA} , its results $\mathbf{z}'_{\xi}{}^k$ cannot be simply transformed back to the results \mathbf{z}_{ϕ}^k given by ϕ_{VPA} in \mathcal{O} , namely, $\mathcal{T}_{L^{-1}} \mathbf{z}'_{\xi}{}^k \neq \mathbf{z}_{\phi}^k$. In other words, if observing in \mathcal{O} , the VPA carried out in different reference frames $\mathcal{T}_{L^{-1}} \circ \xi_{VPA} \mathbf{z}'{}^0$ and $\phi_{VPA} \mathbf{z}^0$ are actually two different algorithms with different properties and outputs. With the same field configuration and initial conditions, the results from ξ_{VPA} and ϕ_{VPA} are shown in Fig. 3. If $\Delta t = 0.1$, see Fig. 3c, the position difference of orbits in Fig. 3a and b is in the order of $R_0 \sim 10^{-3}$ m. If $\Delta t = 0.628$, see Fig. 3e, $\mathcal{T}_{L^{-1}} \circ \xi_{VPA} \mathbf{z}'{}^0$ becomes unstable and gives wrong numerical results. Similarly, the non-covariant property of NCOVA is shown in Fig. 4. When applied in different frames, NCOVA also becomes different algorithms and hence has different performances, see numerical results $\phi_{NCOVA} \mathbf{z}^0$ and $\mathcal{T}_{L^{-1}} \circ \xi_{NCOVA} \mathbf{z}'{}^0$ in Fig. 4a, b, d, and e. The D_x is also comparable to the value of R_0 and dependent with the step-length, see Fig. 4e, f. According to Figs. 3 and 4, the non-covariant problem results from the non-covariant algorithms in different Lorentz frame are well exhibited.

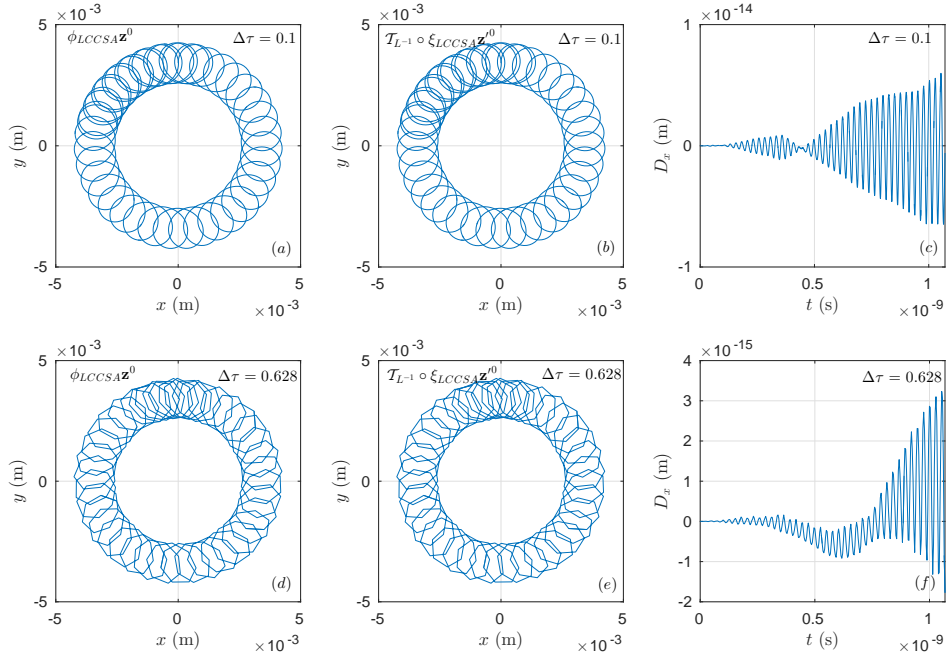


Figure 2. The comparison of simulation results are given by LCCSA in different Lorentz frames. Subfigures a, b and c are simulated with the step-length $\Delta\tau = 0.1$, while subfigures d, e and f are calculated by $\Delta\tau = 0.628$. The difference between the results calculated in two frames is in the order of machine precision, which caused by the imprecision of Lorentz transformation instead of the algorithm itself.

B. The secular stability

All LCCSAs possess good long-term properties belonging to standard symplectic algorithms. The covariant Hamiltonian in Eq.31, known as the mass-shell, is a constant of motion. Through conserving the symplectic structure, LCCSA can restrict the global error of the mass-shell under a small value [17]. For comparison, we develop a Lorentz covariant but non-symplectic algorithm, i.e., a fourth-order Runge-Kutta method (RK4), to solve the 4-dimensional covariant Lorentz equations,

$$\frac{dX^\alpha}{d\tau} = U^\alpha, \quad (43)$$

$$\frac{dp^\alpha}{d\tau} = F^{\alpha\beta}U_\beta, \quad (44)$$

where p^α is the 4-mechanical-momentum, U^α is the 4-velocity, and $F^{\alpha\beta}$ is the electromagnetic tensor [18]. We can see that RK4 is a Lorentz covariant algorithm because its discretization

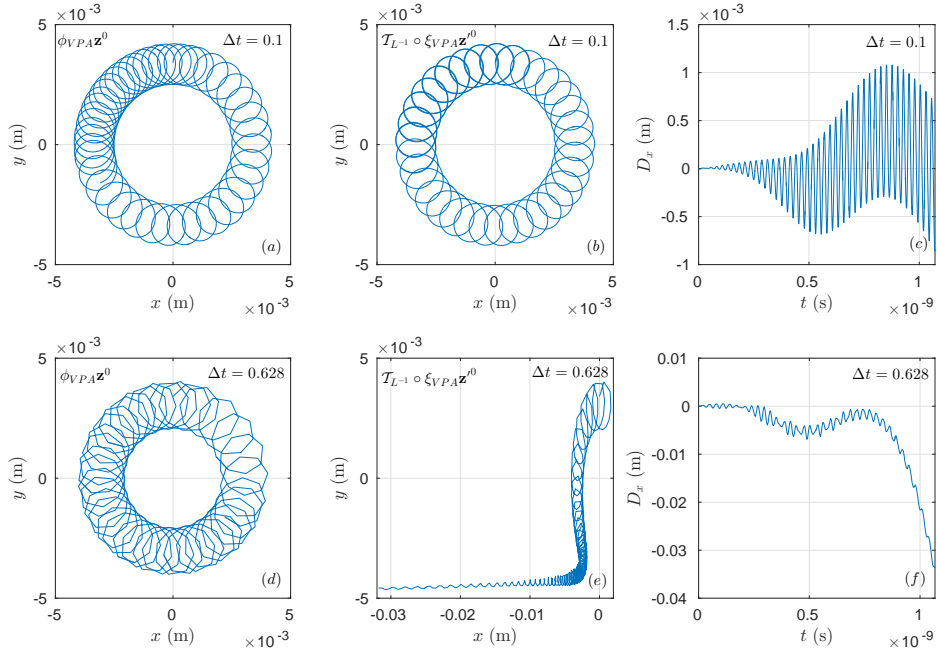


Figure 3. The comparison of simulation results are given by VPA in different Lorentz frames. Subfigures a, b and c are simulated with the step-length $\Delta t = 0.1$, while subfigures d, e and f are calculated with $\Delta t = 0.628$. The position difference between the numerical results in two frames is comparable to R_0 with $\Delta t = 0.1$. The VPA applied in the frame \mathcal{O}' turns out unstable with $\Delta t = 0.628$.

does not break the geometric structure of Eqs. 43 and 44.

Figure 5 compares the evolutions of relative numerical error of mass-shell calculated by RK4 and the LCCSA. The electromagnetic field and initial conditions are set the same as in Fig. 2, and the step-length is set to be $\Delta\tau = 0.1$. After 2×10^6 proper-time steps, the relative mass-shell error of RK4 accumulates to a significant value, which results in unreliable numerical results. However, the relative error of LCCSA keeps bounded in a small region due to its symplectic nature. According to this numerical experiment, Lorentz covariant algorithms without secular conservativeness suffer from coherent accumulation of numerical errors, which implies the necessity to combine the Lorentz covariance and the structure-preserving methods.

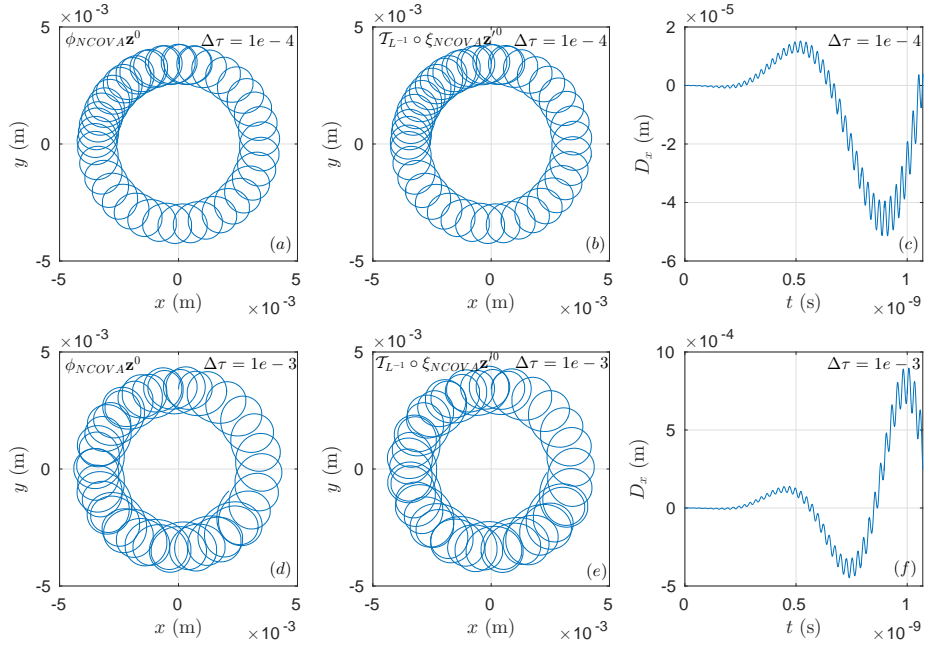


Figure 4. The comparison of simulation results are given by NCOVA in different Lorentz frames. Subfigures a, b and c are simulated with the step-length $\Delta\tau = 0.0001$, while subfigures d, e and f are calculated with $\Delta\tau = 0.001$. The NCOVA is a 1st-order non-covariant algorithm and does not preserve symplectic structure. The time step-length required for stability is much smaller than LCCSA. The inconsistency between the results calculated in different frames is comparable to R_0 though with small time steps.

C. The energy-based adaptive time step

Through the discretization of the proper time τ , LCCSA also possesses built-in energy-based adaptive-time-step property. The discrete relation between $\Delta\tau$ and Δt can be reflected by the 0th component of Eq. 37 as

$$\Delta t = t^{k+1} - t^k = \Delta\tau \left(P_0^{k+1} - \phi^k \right), \quad (45)$$

where P_0 is the 0th component of canonical momentum, and ϕ is the electric potential. Considering that the expression in the bracket of Eq. 45 can be rewritten as $P_0^{k+1} - \phi^k = \gamma^{k+1} + \phi^{k+1} - \phi^k$ and $\Delta\phi = \phi^{k+1} - \phi^k$ generally is a small value, the time step Δt is approximately proportional to γ^{k+1} . Equation 45 is actually a discrete version of the relation $dt = \gamma d\tau$. For constant $\Delta\tau$, the time step Δt can be self-adapted according to the energy

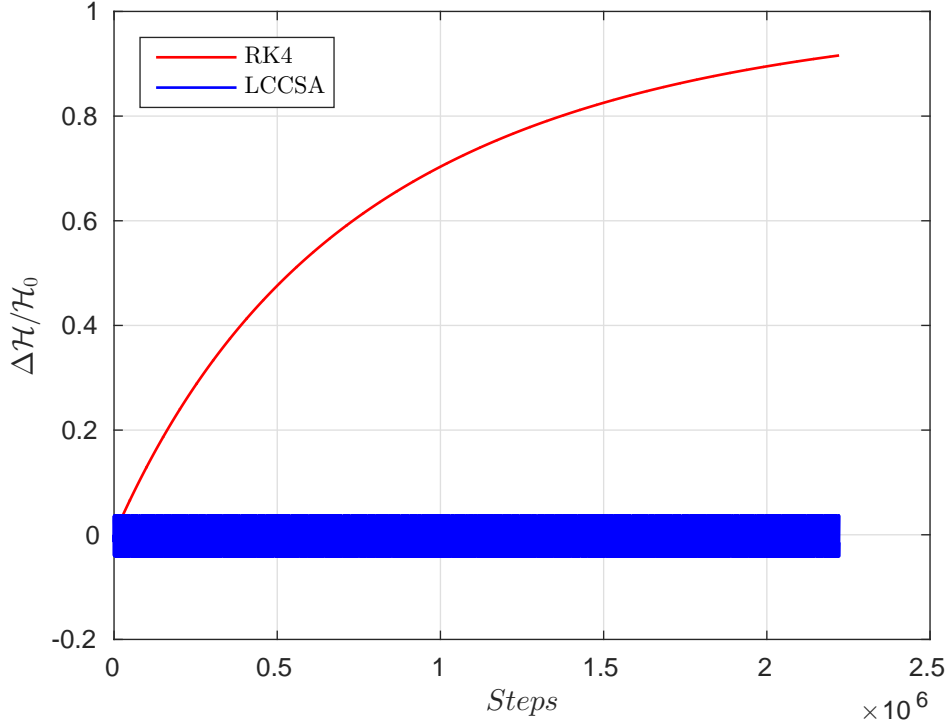


Figure 5. The evolutions of relative errors of mass-shell by RK4 and LCCSA. The step-length is $\Delta\tau = 0.1$. The error of mass-shell given by RK4 becomes comparable to \mathcal{H}_0 after 2×10^6 steps, while the relative error is limited under a small value in the case of LCCSA.

of particles. When a charged particle moves in an external magnetic field, the gyro-period $T_{ce} = 2\pi\gamma m_0/eB$ determines the smallest time-scale of the particle dynamics. In simulations, to resolve the dynamical behaviors smaller than the time-scale of gyro-period, the time step should be restricted smaller than T_{ce} . When considering the efficiency of computation, too small time step brings heavy computation consuming. One should choose a suitable Δt to balance the accuracy and the efficiency. Because T_{ce} is proportional to γ , for algorithms with fixed time step Δt , time steps lie in one gyro-period grows as the increase of γ , which cause the waste of calculation resources in problems with increasing γ . On the other hand, if the particle loses energy quickly in some processes, T_{ce} may drop to smaller than Δt , which results in numerical instabilities for algorithms. However, the time-step problems can be avoided easily by using the LCCSA.

To show the advantages of the energy-based adaptive time steps, the acceleration and braking process of an electron is simulated in a uniform magnetic field. We compare the

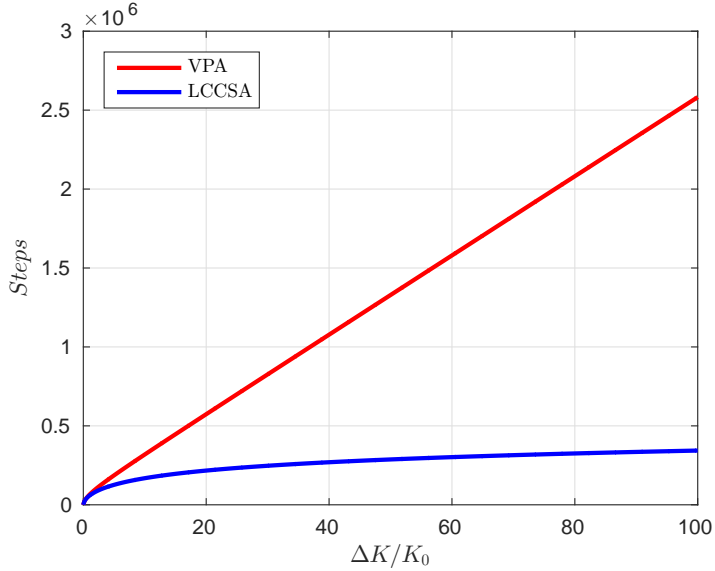


Figure 6. The numbers of simulation steps in terms of the relative increase of energy required by VPA and LCCSA to simulate the same acceleration process of an electron.

performance of LCCSA with VPA which has a fixed time step [13]. Both the electric and magnetic fields have only z-component, namely, $\mathbf{B} = B_0 \mathbf{e}_z$ and $\mathbf{E} = E_0 \mathbf{e}_z$. In the acceleration process, the particle is released at $x = 1.8$ m, $y = z = 0$, the magnetic field is set as $B_0 = 2$ T, and the electric field is $E_0 = 10000$ V/m. The initial momentum of the electron is given by $\mathbf{p}_0 = (0, 1 m_0 c, 0.1 m_0 c)$. Figure 6 shows the number of steps iterated by VPA and LCCSA in terms of different relative increments of kinetic energy. As the increase of the energy, the slope of red curve keeps unchanged, while the slope of blue curve decreases significantly, see Fig. 6. Therefore, to reach the same energy, the computation efficiency of LCCSA is much better than VPA. In the case of braking process, the initial position and the magnetic field are the same as before, the electric field is set as $E_0 = 1$ MV/m, and the initial momentum is given by $\mathbf{p}_0 = (0, 1 m_0 c, -10 m_0 c)$. Figure 7 depicts the number of time samplings during each gyro-period. The sampling number of VPA in one gyro-period decreases as the decrease of energy due to the fixed time step, while the time sampling number of LCCSA keeps unchanged. In this case, through adjusting the time step automatically, LCCSA can provide higher accuracy than VPA and avoid numerical instabilities in the simulation of energy decrease processes.

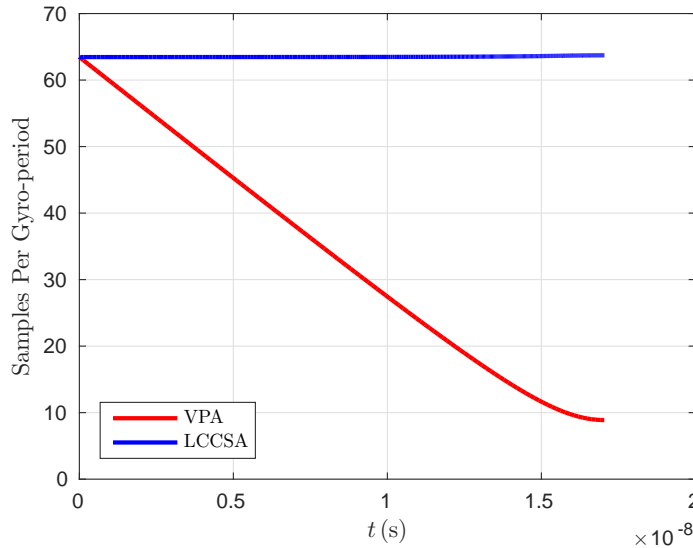


Figure 7. Numbers of time steps in one gyro-period when employing VPA and LCCSA to simulate the same decelerate process of an electron. As the decrease of the energy, the number of time-samplings in one gyro-period for LCCSA keeps unchanged, while the number of time-samplings for VPA decreases.

V. CONCLUSIONS

In this paper, we provide the definition of Lorentz covariant algorithms and introduce Lorentz covariant symplectic algorithms in detail. Lorentz covariant algorithms can generate discretized equations, which inherits the Lorentz covariant nature of original continuous systems. Symplectic algorithms without Lorentz covariance only performs well in one specific inertial frame. While covariant symplectic algorithms are reference-independent and possess long-term conservativeness, which make it convenient and safe to employ the same algorithm in any Lorentz frame. Because of the essentiality of Lorentz covariance, the Lorentz covariant symplectic algorithms have wide applications.

On the other hand, because the time-variable becomes a component of coordinate for 4-spacetime in the construction of LCCSA, the time-dependent Hamiltonian system is no longer a problem for the construction of required symplectic algorithms. Taking the proper time τ as the dynamical parameter, all time-dependent Hamiltonian system becomes proper-time-independent. The explicit symplectic algorithm, like the LCCSA in Eqs. 36-37, for time dependent systems can be easily constructed. According to the idea and procedure in this

paper, many other Lorentz covariant symplectic algorithms as well as other kinds of Lorentz covariant structure-preserving algorithms can be readily constructed. In the future work, we will further investigate the Lorentz covariant structure-preserving algorithms and apply the LCCSAs to study key physical problems.

ACKNOWLEDGMENTS

This research is supported by National Magnetic Confinement Fusion Energy Research Project (2015GB111003, 2014GB124005), National Natural Science Foundation of China (NSFC-11575185, 11575186, 11305171), JSPS-NRF-NSFC A3 Foresight Program (NSFC-11261140328), Key Research Program of Frontier Sciences CAS (QYZDB-SSW-SYS004), and the GeoAlgorithmic Plasma Simulator (GAPS) Project.

-
- [1] H. Qin and X. Guan, *Phys. Rev. Lett.* **100**, 035006 (2008).
 - [2] H. Qin, X. Guan, and W. M. Tang, *Phys. Plasmas* **16**, 042510 (2009).
 - [3] J. Li, H. Qin, Z. Pu, L. Xie, and S. Fu, *Phys. Plasmas* **18**, 052902 (2011).
 - [4] X. Guan, H. Qin, and N. J. Fisch, *Phys. Plasmas* **17**, 092502 (2010).
 - [5] J. Liu, H. Qin, N. J. Fisch, Q. Teng, and X. Wang, *Phys. Plasmas* **21**, 064503 (2014).
 - [6] J. Xiao, J. Liu, H. Qin, and Z. Yu, *Phys. Plasmas* **20**, 102517 (2013).
 - [7] J. Xiao, J. Liu, H. Qin, Z. Yu, and N. Xiang, *Phys. Plasmas* **22**, 092305 (2015).
 - [8] J. Xiao, H. Qin, J. Liu, Y. He, R. Zhang, and Y. Sun, *Phys. Plasmas* **22**, 112504 (2015).
 - [9] H. Qin, J. Liu, J. Xiao, R. Zhang, Y. He, Y. Wang, Y. Sun, J. W. Burby, L. Ellison, and Y. Zhou, *Nucl. Fusion* **56**, 014001 (2015).
 - [10] J. Liu, Y. Wang, and H. Qin, *Nucl. Fusion* **56**, 064002 (2016).
 - [11] Y. Wang, H. Qin, and J. Liu, *Physics of Plasmas* **23**, 062505 (2016).
 - [12] Y. He, Y. Sun, J. Liu, and H. Qin, *J. Comput. Phys.* **281**, 135 (2015).
 - [13] R. Zhang, J. Liu, H. Qin, Y. Wang, Y. He, and Y. Sun, *Phys. Plasmas* **22**, 044501 (2015).
 - [14] Y. He, Y. Sun, J. Liu, and H. Qin, *J. Comput. Phys.* **305**, 172 (2016).
 - [15] Y. He, H. Qin, Y. Sun, J. Xiao, R. Zhang, and J. Liu, *Phys. Plasmas* **22**, 124503 (2015).
 - [16] R. Zhang, J. Liu, Y. Tang, H. Qin, J. Xiao, and B. Zhu, *Phys. Plasmas* **21**, 032504 (2014).

- [17] E. Hairer, C. Lubich, and G. Wanner, *Geometric numerical integration: structure-preserving algorithms for ordinary differential equations*, vol. 31 (Springer Science & Business Media, 2006), ISBN 3540306668.
- [18] J. D. Jackson, *Classical electrodynamics*, vol. 3 (Wiley New York etc., 1962).
- [19] H. Qin, Report, Princeton Plasma Physics Lab., Princeton, NJ (US) (2005).
- [20] H. Qin, R. Cohen, W. Nevins, and X. Xu, *Phys. Plasmas* **14**, 056110 (2007).
- [21] H. Goldstein, *Classical mechanics* (Pearson Education India, 1965), ISBN 8131758915.